Optimal Power Flow Using an Extended Conic Quadratic Formulation

Rabih A. Jabr, *Member, IEEE*

***Abstract*—Recent research has shown that the load flow equations describing the steady-state conditions in a meshed network can be placed in extended conic quadratic (ECQ) format. This paper presents a study of the implementation of the new load flow equations format in an optimal power flow (OPF) program which accounts for control devices such as tap-changing transformers, phase-shifting transformers, and unified power flow controllers. The proposed OPF representation retains the advantages of the ECQ format: 1) it can be easily integrated within optimization routines that require the evaluation of second-order derivatives, 2) it can be efficiently solved for using primal-dual interior-point methods, and 3) it can make use of linear programming scaling techniques for improving numerical conditioning. The ECQ-OPF program is employed to solve the economic dispatch and active power loss minimization problems. Numerical testing is used to validate the proposed approach by comparing against solution methods and results of standard test systems.**

***Index Terms*—Load flow control, nonlinear programming, optimization methods.**

I. Introduction

THE optimal power flow (OPF) is an essential tool for the economic planning and operation of both vertically integrated and restructured power systems. Research into OPF solution techniques has been active since the problem was first studied by Carpentier in 1962 [1]. Current OPF programs are expected to accurately account for classical load flow control devices such as tap-changing/phase-shifting transformers and modern flexible ac transmission systems (FACTS). It is understood herein that the OPF formulation models the network using the full ac representation.

The most popular OPF techniques can be classified as either active set or path-following interior-point methods. Active set methods include the Lagrange–Newton method [2], sequential quadratic programming (SQP) [3], simplex based sequential linear programming (SLP) [4], [5], and the method of feasible directions [6]. The main difficulty in the active set methods lies in the identification of the binding inequality constraints at optimality. In essence, these methods have to generate a guess of the active set at every iteration and test it for feasibility and/or optimality. This is unlike path-following interior-point methods [7] where the active set is determined asymptotically as the solution is approached. The power systems literature reports applications of several enhancements over the pure path-following primal-dual interior-point method [8]: 1) Mehrotra's predictor-corrector technique [9]–[12], 2) Gondizio's multiple-centrality corrections [13], [14], 3) trust region technique [15], and 4) optimal step length control [16], [17]. A comprehensive survey of OPF techniques published prior to 1993 is given in [18] and [19]. A more recent review including FACTS devices appears in [20].

Despite the myriad of OPF solution methods which account for an ac network model, DC-OPF methods are still employed for administering market rules in deregulated industries [21]. Linear programming algorithms for solving the DC-OPF problem always yield solutions at the expense of simplified network modeling that ignores voltage and reactive power constraints. The case against the use of OPF methods for real-time operation is that the nonlinear programming methods are less numerically robust than their linear programming counterparts and are prone to convergence problems. Further research is required to overcome these concerns.

This paper presents an interior-point based OPF code in which the constraints are modeled using an extended conic quadratic (ECQ) format. In retrospect, previous research on interior-point OPF programs reported the use of the voltage polar coordinates model [8], [9], [12], [16], [17], the voltage rectangular model [10], [11], [13], and the current mismatch formulation [22]. The ECQ model of the meshed power network equations was first proposed in [23]. It is an extension of the conic quadratic model of radial networks [24], [25]. [25] shows that the radial load flow equations can be efficiently solved using an interior-point method for convex conic quadratic programming. This transformation to a convex program is possible because equations which explicitly refer to interrelations between voltage angles are not required in the conic quadratic model of radial networks. The same does not hold true for meshed networks [23]. Therefore, the ECQ model for meshed networks, akin to the classical ac network power flow model, results in an OPF problem with a nonconvex feasible region. Nevertheless, the ECQ-OPF is amenable to solution using primal-dual interior-point methods. In the ECQ-OPF model, the power flow and injection expressions are all linear. The nonlinearity in the classical power flow model is transferred into a set of rotated conic quadratic and arctangent equality constraints. The advantages of this model are the following.

1) The nonzero entries of the Lagrangian Hessian matrix correspond only to the set of rotated conic quadratic and arctangent constraints. This holds true even for networks with power injection models of tap-changing transformers [12], phase-shifters [12], and unified power flow controller (UPFC) devices [26], [27]. The Hessian matrix can be therefore easily integrated within

Manuscript received August 22, 2007; revised January 14, 2008. Paper no. TPWRS-00600-2007.

The author is with the Electrical, Computer, and Communication Engineering Department, Notre Dame University, Zouk Mosbeh, Lebanon (e-mail: rjabr@ndu.edu.lb).

Digital Object Identifier 10.1109/TPWRS.2008.926439

optimization procedures that require second-order derivatives such as primal-dual interior-point methods.

2) The linearity of the power injection equations and load flow controller models allows the use of linear programming scaling techniques [28] for improving the numerical conditioning of the problem.

The proposed OPF is tested with two different objective functions: 1) power generation cost with quadratic cost curves and 2) active power loss. Simulations are reported on systems with up to 2383 buses. Comparisons are carried out with results published in [26], [29]–[31] and also with solutions obtained from MINOS [32] and PDIPM [17] used in MATPOWER [33].

II. Extended Conic Quadratic Load Flow Format

Consider an N-bus interconnected power system operating in steady-state and under normal conditions. The system is assumed to be balanced and is represented by its single-phase network with all quantities specified in per unit on a common MVA base. Let $\hat{Y}_{in} = G_{in} + jB_{in}$ denote the complex rectangular representation of an element in the bus admittance matrix. If bus voltages are expressed in polar form ($\tilde{V}_i = V_i \angle \theta_i$), the real and reactive injected power at an arbitrary bus i are given by [34]

$$P_i = V_i^2 G_{ii} + \sum_{\substack{n=1 \\ n\neq i}}^{N} [V_i V_n G_{in} \cos(\theta_i - \theta_n) + V_i V_n B_{in} \sin(\theta_i - \theta_n)] \tag{1}$$

$$Q_i = -V_i^2 B_{ii} - \sum_{\substack{n=1 \\ n\neq i}}^{N} [V_i V_n B_{in} \cos(\theta_i - \theta_n) - V_i V_n G_{in} \sin(\theta_i - \theta_n)]. \tag{2}$$

By following [23], define

$$R_{in} = V_i V_n \cos(\theta_i - \theta_n) \tag{3}$$

$$T_{in} = V_i V_n \sin(\theta_i - \theta_n) \tag{4}$$

$$u_i = \frac{V_i^2}{\sqrt{2}}. \tag{5}$$

The nonlinear power flow equations become

$$P_i = \sqrt{2} G_{ii} u_i + \sum_{\substack{n=1 \\ n\neq i}}^{N} [G_{in} R_{in} + B_{in} T_{in}] \tag{6}$$

$$Q_i = -\sqrt{2} B_{ii} u_i - \sum_{\substack{n=1 \\ n\neq i}}^{N} [B_{in} R_{in} - G_{in} T_{in}]. \tag{7}$$

From definitions (3)–(5), it follows that

$$2u_i u_n = R_{in}^2 + T_{in}^2 \tag{8}$$

$$\theta_i - \theta_n = \tan^{-1}\left(\frac{T_{in}}{R_{in}}\right). \tag{9}$$

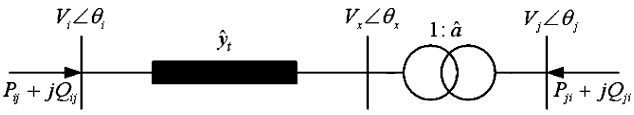

Fig. 1. Regulating transformer equivalent circuit.

For radial networks, (6)–(8) are sufficient to describe the load flow solution model [24], [25]. As shown in [25], these equations are compatible with the conic quadratic (CQ) format because 1) (6) and (7) are linear and 2) the objective of the CQ model can be set such that the rotated conic quadratic (8) equality constraints can be transformed into inequality constraints which define a convex set. The feasible region in the CQ model therefore includes the intersection of the convex sets formed of linear equality constraints and nonlinear inequality constraints. For meshed networks, the arctangent equalities (9) are also required to completely specify the load flow model [23]. However, trigonometric functions are not compatible with the classical CQ format [35]. Equations (6)–(9) are therefore referred to as the extended conic quadratic format of the load flow equations. The feasible region of the ECQ model is nonconvex. In the ECQ format, it is understood that the angle at the slack bus is zero and both u_i and R_{in} take only nonnegative values. The bus voltage magnitudes can be deduced from the ECQ variables by solving (5)

$$V_i = (\sqrt{2} u_i)^{1/2}. \tag{10}$$

III. Power Injection Models of Load Flow Controllers

The ECQ load flow equations can be modified to account for load flow controllers represented via their power injection models. In this work, three types of controllers are considered: the tap-changing transformer, the phase-shifting transformer, and the UPFC. Both the tap-changing/voltage regulating and phase-shifting transformers can be accounted for using the regulating transformer model.

A. Regulating Transformer Model

A regulating transformer is a device that can regulate real and reactive power flows in a network [34]. Its modeling in a Newton OPF is described in detail in [29]. Consider a regulating transformer with admittance $\hat{y}_t$ in series with an ideal transformer representing the complex tap ratio $1 : \hat{a}$ as shown in Fig. 1. The admittance $\hat{y}_t$ is based on the nominal ratio, i.e., $\hat{a} = 1$ [34]. Since the complex power on either side of the ideal transformer is the same, the equivalent power injection model of the regulating transformer can be represented as in Fig. 2 with the quantities at the fictitious bus x constrained as follows [12]:

$$a^{\min} \leq \frac{V_j}{V_x} \leq a^{\max} \tag{11}$$

$$\phi^{\min} \leq \theta_j - \theta_x \leq \phi^{\max}. \tag{12}$$

In the above equations, $[a^{\min}, a^{\max}]$ and $[\phi^{\min}, \phi^{\max}]$ are the intervals for the magnitude and angle of the complex tap ratio $\hat{a} = a\angle\phi$. The tap-changing (or voltage regulating) transformer

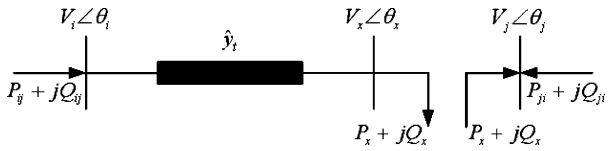

Fig. 2. Regulating transformer power injection model.

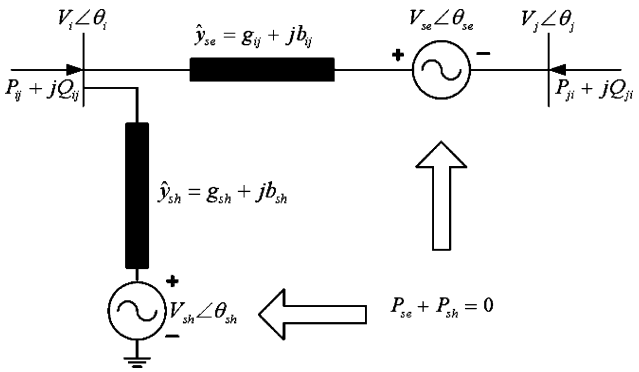

Fig. 3. UPFC equivalent circuit.

model can be obtained by setting $\phi^{\min} = \phi^{\max} = 0$. Similarly, $a^{\min} = a^{\max} = 1$ results in the phase-shifter model.

Equation (11) can be easily placed in a form compatible with the ECQ programming model. By using (5) for V_j and V_x, (11) becomes

$$(a^{\min})^2 u_x \le u_j \le (a^{\max})^2 u_x. \tag{13}$$

Equation (12) is already in the ECQ format. As depicted in Fig. 2, the lossless ideal transformer model requires that the real/reactive power extracted from bus x is injected into bus j. It is possible to account for this constraint without introducing the additional variables P_x and Q_x. This can be done by combining buses x and j into one super-node and writing the real/reactive injection (6)-(7) at this node. The result is equivalent to adding the real/reactive injection equation at bus x to the real/reactive injection equation at bus j.

B. UPFC Model

One of the most comprehensive FACTS devices is the unified power flow controller. When fixed at one end of a line, the UPFC can be used to simultaneously control the bus voltage magnitude, the real power line flow, and the reactive power line flow [29].

The principle of operation of the UPFC is well documented in the power systems literature [20], [29]. Its equivalent circuit under steady-state operating conditions is given in Fig. 3. The equivalent circuit includes two voltage sources operating at the fundamental frequency and two impedances. The voltage sources represent the fundamental Fourier series component of the ac converter output voltage waveforms whereas the impedances model the resistances and leakage inductances of the coupling transformers [29].

References [36] and [31] discuss Newton and interior-point methods for including the UPFC in OPF studies. In these implementations, the UPFC control parameters (voltage magnitude and angle in the series and shunt converters) are treated as independent variables in the optimization process. This comprehensive modeling is at the expense of having the success of the iterative solution sensitive to the choice of the initial UPFC control parameters. For the Newton OPF, [36] proposes an initialization procedure which aims to produce good UPFC initial conditions. Another promising representation is the power injection model proposed by Handschin and Lehmköster [26]. This model is a strict linear representation of the UPFC and therefore does not contribute to the nonconvexity of the power flow equations [27]. Moreover, it does not suffer from problems related to initial point selection. References [26] and [27] test the use of the UPFC PIM in a SQP based OPF implementation.

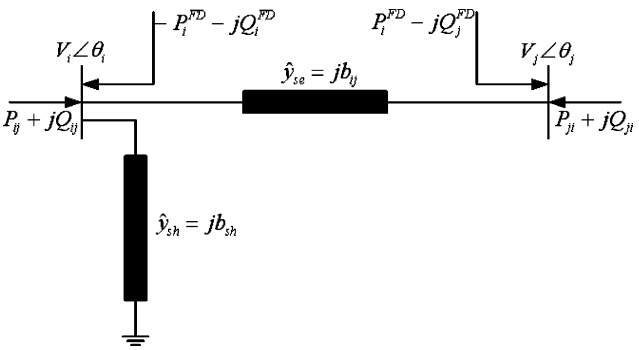

Fig. 4. UPFC power injection model.

By neglecting the resistances of the coupling transformers and assuming lossless converter valves, the UPFC equivalent circuit can be represented by its power injection model (PIM) given in Fig. 4 [26], [27]. In the PIM, the power injection quantities P_i^{FD}, Q_i^{FD}, and Q_j^{FD} are treated as additional independent variables. The UPFC real power injection into bus j, $-P_j^{FD}$, is equal to P_i^{FD}. The injections in the UPFC PIM are related to the quantities in the equivalent circuit in Fig. 3 as follows:

$$P_i^{FD} = -V_i V_{se} b_{ij} \sin(\theta_i - \theta_{se}) - V_i V_{sh} b_{sh} \sin(\theta_i - \theta_{sh}) \tag{14}$$

$$Q_i^{FD} = V_i V_{se} b_{ij} \cos(\theta_i - \theta_{se}) + V_i V_{sh} b_{sh} \cos(\theta_i - \theta_{sh}) \tag{15}$$

$$P_j^{FD} = V_j V_{se} b_{ij} \sin(\theta_j - \theta_{se}) \tag{16}$$

$$Q_j^{FD} = -V_j V_{se} b_{ij} \cos(\theta_j - \theta_{se}). \tag{17}$$

The UPFC PIM can be directly integrated into the ECQ load flow equations by 1) including the series and shunt coupling transformers into the bus admittance matrix computation and 2) adding the UPFC injection quantities as additional variables. Equations (14)–(17) can be used to define upper and lower bounds on each of the UPFC injections. The voltage magnitude and angle of the series and shunt voltage sources in Fig. 3 can be deduced from the UPFC PIM by solving (14)–(17). The closed-form solution is

$$V_{se} = \frac{-\sqrt{(P_j^{FD})^2 + (Q_j^{FD})^2}}{V_j b_{ij}} \tag{18}$$

$$\theta_{se} = \theta_j - \operatorname{atan2}(-P_j^{FD}, Q_j^{FD}) \tag{19}$$

$$V_{sh} = \frac{-\sqrt{\left(P_i^{FD1}\right)^2 + \left(Q_i^{FD1}\right)^2}}{V_i b_{sh}} \quad (20)$$

$$\theta_{sh} = \theta_i - \text{atan2}(P_i^{FD1}, Q_i^{FD1}). \quad (21)$$

In the above equations, atan2 is the four-quadrant arctangent function and

$$P_i^{FD1} = P_i^{FD} + V_i V_{se} b_{ij} \sin(\theta_i - \theta_{se}) \quad (22)$$

$$Q_i^{FD1} = -Q_i^{FD} + V_i V_{se} b_{ij} \cos(\theta_i - \theta_{se}). \quad (23)$$

IV. Optimal Power Flow

A. Formulation

Two objectives are considered, minimum generation cost

$$\text{minimize} \sum_i c_{0i} + c_{1i} P_{gi} + c_{2i} P_{gi}^2 \quad (24)$$

and minimum active power loss

$$\text{minimize } P_s. \quad (25)$$

In the above equations, P_{gi} is the power supplied by a generator connected to bus i, c_{0i}, c_{1i}, and c_{2i} are the corresponding cost curve coefficients, and P_s is the real power injected into the slack bus. It is also straightforward to model convex piecewise-linear cost curves which appear in market operation by using interpolatory variables [12].

The minimization of any of the above objectives is subject to physical and technical constraints. Most importantly, a meaningful OPF solution should satisfy the real and reactive power injection constraints (6) and (7) and the feasibility constraints (8) and (9). The injected powers in (6) and (7) are

$$P_i = P_{gi} - P_{di}, \text{ and} \quad (26)$$

$$Q_i = Q_{gi} - Q_{di} + Q_{ci} \quad (27)$$

where P_{gi}/Q_{gi} is the real/reactive power generated at bus i, P_{di}/Q_{di} is the real/reactive power demand of the load at bus i, and Q_{ci} is the reactive power injected by a capacitor at bus i. The generated power needs to satisfy technical limits on the minimum and maximum values of generation

$$P_{gi}^{\min} \le P_{gi} \le P_{gi}^{\max}, \text{ and} \quad (28)$$

$$Q_{gi}^{\min} \le Q_{gi} \le Q_{gi}^{\max}. \quad (29)$$

However, for the problem of active loss minimization (25), P_{gi} is set to a pre-specified value and (28) is dropped from the constraint set. For both objectives (24) and (25), the reactive power constraint (29) is accounted for. Another common OPF constraint relates to the minimum and maximum allowable limits of a bus voltage magnitude. In the ECQ format, this constraint at an arbitrary bus i is

$$\frac{\left(V_i^{\min}\right)^2}{\sqrt{2}} \le u_i \le \frac{\left(V_i^{\max}\right)^2}{\sqrt{2}}. \quad (30)$$

Power flow controllers such as tap-changing/phase-shifting transformers and UPFC devices are included in the ECQ-OPF using the power injection models in Section III. Moreover, the ECQ-OPF can account for target values of voltage magnitudes, real power flows, and reactive power flows set by the controllers. In particular, tap-changers can be employed to control bus voltage magnitudes whereas phase-shifters are used to specify real power flows. On the other hand, the UPFC can set the values of any combination of bus voltage magnitude, real power flow, and reactive power flow. The control targets in the ECQ-OPF are enforced as linear equality constraints. For instance, the following formulae are used for the real and reactive power flows on line i-n and leaving bus i

$$P_{in} = \sqrt{2} g_{in} u_i - g_{in} R_{in} - b_{in} T_{in} \quad (31)$$

$$Q_{in} = -\sqrt{2}\left(b_{in} + \frac{b_{sh}}{2}\right) u_i + b_{in} R_{in} - g_{in} T_{in} \quad (32)$$

where g_{in} and b_{in} are the series conductance and susceptance in the π equivalent model and $b_{sh}/2$ is the ½ charging susceptance. Equation (31) can be also used to limit the power flow on an arbitrary line in accordance with its power transmission capability [34]. Alternatively, it is also possible to limit the (squared) magnitude of the line current using a linear equation [37]

$$I_{in}^2 = \sqrt{2} A u_i + \sqrt{2} B u_n - 2C R_{in} + 2D T_{in} \quad (33)$$

$$\text{where } A = g_{in}^2 + \left(b_{in} + \frac{b_{sh}}{2}\right)^2 \quad (34)$$

$$B = g_{in}^2 + b_{in}^2 \quad (35)$$

$$C = g_{in}^2 + b_{in}\left(b_{in} + \frac{b_{sh}}{2}\right) \quad (36)$$

$$D = \frac{g_{in} b_{sh}}{2}. \quad (37)$$

B. Interior-Point Solver

Except for rotated conic quadratic (8) and arctangent (9) equality constraints, all the other equality and inequality constraints in the ECQ-OPF are linear. Motivated by the success of primal-dual interior point methods for solving conic quadratic programs [35], the solution to the ECQ-OPF formulation was also approached using an interior-point method. The chosen interior-point method employs the popular Mehortra's predictor-corrector technique. Implementation details are documented in [38]. The interior-point solver requires, at each iteration, the computation of the Jacobian and Lagrangian Hessian matrices. The Jacobian matrix corresponding to all constraints except (8) and (9) is constant throughout all iterations. For the feasibility constraints (8) and (9), the formulae for computing the Jacobian and Hessian elements are given in Appendix A. The initial vector is chosen to correspond to a flat start

$$u_i = \frac{1}{\sqrt{2}} \text{ and } \theta_i = 0 \quad \text{for all nodes} \quad (38)$$

$$R_{in} = 1 \text{ and } T_{in} = 0 \quad \text{for all lines} \quad (39)$$

$$P_i^{FD} = Q_i^{FD} = Q_j^{FD} = 0 \quad \text{for all UPFC controllers} \quad (40)$$

$$P_{gi} = \frac{\left(P_{gi}^{\min} + P_{gi}^{\max}\right)}{2} \quad \text{for all generators} \quad (41)$$

$$Q_{gi} = \frac{\left(Q_{gi}^{\min} + Q_{gi}^{\max}\right)}{2} \quad \text{for all generators.} \quad (42)$$

The solver terminates when all the stopping criteria [38] are satisfied with a tolerance of 10^{-8}.

C. Scaling

Scaling of a problem's objective and constraint functions is achieved by multiplying each of the functions by a constant chosen such that the value of each scaled function, evaluated for typical values of the problem variables, is of the same order of magnitude. In SQP algorithms, it is recommended to scale the problem so that the cost function gradient is of similar magnitude to each of the constraint function gradients [39]. Classical scaling in linear programming suggests scaling rows and columns to have unit norms [28].

The numerical experiments conducted on the ECQ programming format have shown that convergence with a reduced number of interior-point iterations can be obtained if 1) the coefficient matrix of linear equations is scaled such that its rows have unit (Euclidean) norm and 2) the objective function is scaled such that it is around the same order of magnitude as the scaled constraints. Specifically, a different scaling factor is used for each of the objective functions in (24) and (25).

1) For the minimum active power loss problem, the injected power at the slack node (25) is substituted by the linear (6). The resulting linear objective function is scaled so that the norm of its row vector of coefficients is one.
2) In the ECQ-OPF with the quadratic cost function (24), the objective function is scaled by

$$s_c = \frac{\|(c_{11}, c_{21}, \ldots, c_{1i}, c_{2i}, \ldots)\|_2}{N_G} \tag{43}$$

where N_G is the number of generating sets. An important by-product of the OPF solution are the locational marginal prices, i.e., the Lagrange multipliers that give the incremental change in generation cost for an incremental increase in the demand at an arbitrary bus i. However, the Lagrange multipliers of the scaled problem (λ_i^s) are different from those of the original un-scaled problem (λ_i).The Lagrange multiplier of the un-scaled problem in monetary units per MWh is

$$\lambda_i = \frac{1}{S_B}\frac{s_c}{s_{ri}}\lambda_i^s \tag{44}$$

where s_{ri} denotes the scale factor of a row corresponding to the linear real power injection at bus i (6) and S_B is the system base MVA.

D. Software Implementation

A prototype implementation of the ECQ-OPF method was programmed in MATLAB running on an Intel® Core™2 Duo Processor T5300 (1.73 GHz) PC with 1 GB RAM.

V. Numerical Performance and Validation

The performance of the proposed OPF was compared against numerical results and solution techniques reported in [26], [29]–[31]. In all the methods which were compared with, the OPF problems are formulated using the voltage polar coordinates model.

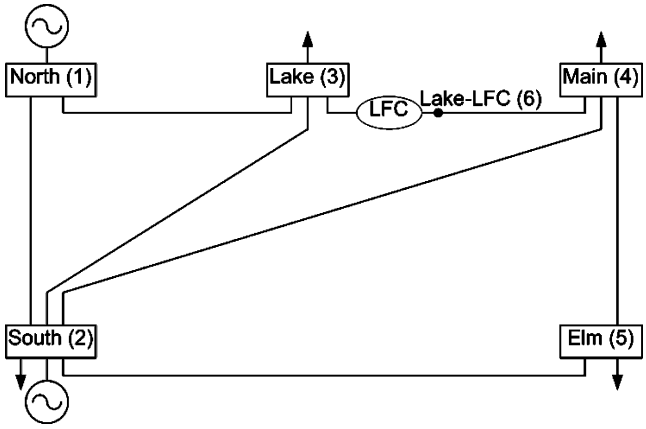

Fig. 5. Benchmark example with one load flow controller.

TABLE I
Nodal Parameters for Case A

Bus	V magnitude [pu]		V angle [deg]		λ [$/MWh]	
	ECQ	[29]	ECQ	[29]	ECQ	[29]
1	1.1095	1.109	0.0000	0.000	4.0442	4.044
2	1.1000	1.100	-1.1939	-1.193	4.1009	4.101
3	1.0767	1.076	-4.0985	-4.098	4.2510	4.251
4	1.0791	1.079	-3.1023	-3.102	4.2005	4.201
5	1.0731	1.073	-4.0972	-4.097	4.2509	4.251
6	1.0798	1.079	-2.7057	-2.705	4.2515	4.182

TABLE II
Nodal Parameters for Case B

Bus	V magnitude [pu]		V angle [deg]		λ [$/MWh]	
	ECQ	[29]	ECQ	[29]	ECQ	[29]
1	1.1097	1.109	0.0000	0.000	4.0411	4.0411
2	1.1000	1.100	-1.3322	-1.332	4.1033	4.1033
3	1.0787	1.078	-3.5058	-3.505	4.2222	4.2222
4	1.0776	1.077	-4.0133	-4.013	4.2353	4.2352
5	1.0724	1.072	-4.5082	-4.508	4.2646	4.2645
6	1.0725	1.072	-4.4578	-4.457	4.2641	4.2640
7	1.0780	1.077	-3.8151	-3.815	4.2247	4.2247

A. Five Bus Benchmark Example

The ECQ-OPF code was initially validated by comparing with published results of a Newton OPF applied to a benchmark 5 bus numerical example [29]. The data for this example are for convenience repeated in Appendix B. Fig. 5 shows the one-line diagram of the network with one load flow controller (LFC) installed in series with the transmission line connecting bus 3 to bus 4. Tables I–III show the nodal parameters (bus voltage magnitudes, phase angles, and Lagrange multipliers) at the optimum point produced by the ECQ-OPF and under three different cases. For validation purposes, the tables also include the nodal parameters as published in [29].

1) Case A (Phase Shifter With Active Power Flow Regulation at Bus 6—Table I): The LFC in Fig. 5 is a phase-shifting transformer with its phase-shift side at bus 3. The feasible range of the phase-shift is in the interval $[-10°, +10°]$. The transformer's winding impedance contains no resistance and a leakage reactance of 0.05 pu. The phase shifter is used to regulate the active power flow through bus 6 at 25 MW. The ECQ-OPF solution gives a cost of 748.330 \$/h with $\phi = -2.009°$ ([29, p. 290]).

TABLE III
NODAL PARAMETERS FOR CASE C

Bus	V magnitude [pu]		V angle [deg]		λ [$/MWh]	
	ECQ	[29]	ECQ	[29]	ECQ	[29]
1	1.0368	1.036	0.0000	0.000	4.0413	4.0412
2	1.0294	1.029	-1.4022	-1.402	4.1078	4.1077
3	1.0000	1.000	-4.6845	-4.685	4.2680	4.2680
4	1.0063	1.006	-3.5807	-3.580	4.2246	4.2246
5	0.9996	0.999	-4.7218	-4.722	4.2823	4.2823
6	1.0072	1.007	-3.1286	-3.128	4.2680	4.2680

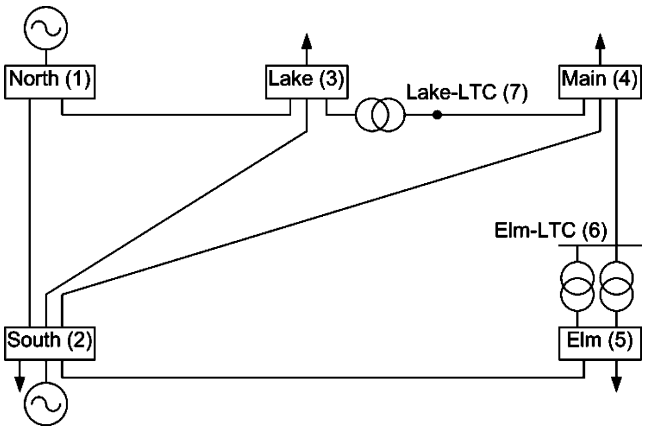

Fig. 6. Benchmark example with three tap-changing transformers.

2) Case B (Three Tap-Changing Transformers—Table II): The five-bus network is modified to include three tap-changing transformers as shown in Fig. 6. The tap-changing sides are assumed to be on buses 3 and 5. The impedances are taken to have no resistance and an inductive reactance of 0.05 pu. The ECQ-OPF solution gives a cost of 747.995 $/h with a tap of 1.002 pu for transformer 3–7 and 1.001 pu for each of the transformers connecting bus 5 to bus 6 ([29, p. 285]).

3) Case C (UPFC—Table III): The LFC in Fig. 5 is a UPFC with its shunt branch at bus 3. Each of the series and shunt winding impedances of the coupling transformers contains no resistance and a leakage reactance of 0.1 pu.

The UPFC was initially simulated under normal operation, i.e., it was used to adjust the active and reactive powers leaving bus 6, towards bus 4, at 25 MW and -6 MVAR, respectively. Moreover, the UPFC shunt converter was set to regulate the bus voltage magnitude at bus 3 at 1 pu. The ECQ-OPF solution sets the UPFC injection quantities in the PIM to the following:

$$P_i^{FD} = -P_j^{FD} = 52.349 \text{ MW},\ Q_i^{FD} = -997.716 \text{ MVAR}$$
$$Q_j^{FD} = -1.649 \text{ MVAR}.$$

Using (18)–(21), the corresponding values of the series and shunt voltage sources are

$$\tilde{V}_{se} = 0.052\angle -94.933^\circ \text{pu},\ \tilde{V}_{sh} = 0.998\angle -4.705^\circ \text{pu}.$$

The corresponding cost is 750.357 $/h ([29, p. 306]).

In addition to the normal UPFC operation discussed above, the ECQ-OPF was tested under various UPFC operating modes: with fixed voltage at bus 3, with fixed real and reactive power flow regulation through bus 6, and with all constraints deactivated. Table IV shows a comparison between the generation cost and power loss obtained by the ECQ-OPF and reported in [29].

TABLE IV
UPFC OPERATING MODES

Operating mode	Generation cost [$/h]		Power loss [MW]	
	ECQ	[29]	ECQ	[29]
Normal UPFC operation	750.357	750.357	3.631	3.631
Fixed voltage at bus 3	749.924	749.928	3.519	3.519
Fixed P and Q	748.236	748.236	3.120	3.119
All constraints deactivated	747.828	747.828	3.015	3.015

TABLE V
TEST RESULTS—IEEE 30 BUS

Case	Control mode			iterations		time (s)
	UPFC1	UPFC2	UPFC3	[31]	ECQ	ECQ
1	-	-	-	-	12	0.14
2	1	1	1	13	9	0.14
3	2	2	2	11	10	0.12
4	3	3	3	14	10	0.16
5	4	4	4	14	11	0.14
6	1	2	3	14	10	0.14
7	1	3	2	13	9	0.12
8	2	1	3	12	13	0.16
9	2	3	1	13	10	0.14
10	3	1	2	13	9	0.12

In all the above cases, the interior-point solver converged within 0.11 s and required between 6 and 11 iterations.

B. IEEE 30-Bus System

The IEEE 30-bus test system modified by Alsac and Stott [30] is a classical numerical example of an OPF problem with a quadratic generation cost function. The ECQ-OPF was run with the data in [30]. It converged to a solution very close to the one in [30] in 12 iterations and 0.14 s. This test is denoted as case 1 in Table V.

Test cases 2 through 10 were carried out on a modification of the IEEE 30-bus test system with three UPFC devices. The UPFC locations and control settings are given in [31, Table IV]. For each UPFC, four control modes are considered:

— mode 1: control of bus voltage and active and reactive power flow;
— mode 2: control of bus voltage and active power flow;
— mode 3: control of bus voltage and reactive power flow;
— mode 4: control of bus voltage.

Table V shows the performance of the ECQ-OPF as compared to the results in [31] under different combinations of UPFC control modes. The results suggest that the ECQ-OPF requires on average a number of interior-point iterations less than the implementation in [31]. Fig. 7 shows a semi-log plot of the convergence characteristics of cases 1 and 2 as measured by the duality gap. It is known that the duality gap is not expected to get small until the primal and dual problems are very nearly feasible [12]. Both with and without the UPFC devices, the duality gap decreased to a positive value less than 10^{-10}.

C. IEEE 118-Bus System

The IEEE 118-bus test system [40] was solved in [26] for minimum active power loss using a SQP approach. A total of

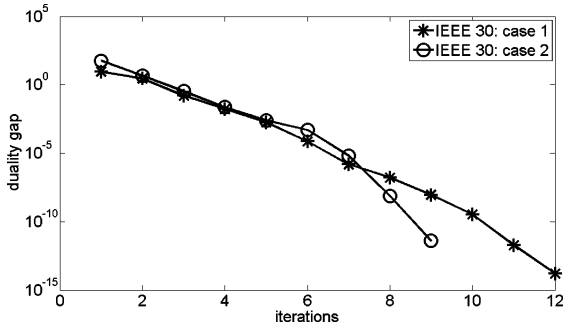

Fig. 7. Duality gap versus the number of iterations for the IEEE 30-bus system.

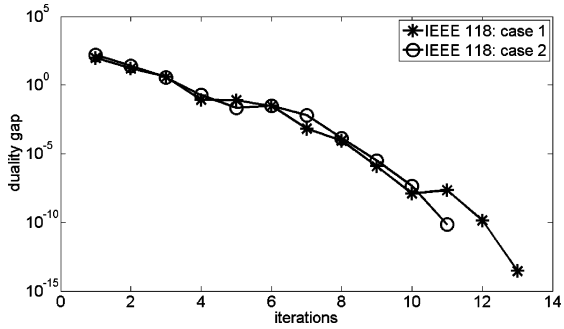

Fig. 8. Duality gap versus the number of iterations for the IEEE 118-bus system.

TABLE VI
TEST RESULTS—IEEE 118 BUS

Case	UPFC in line	Power loss [MW]		iterations		time (s)
		[26]	ECQ	[26]	ECQ	ECQ
1	-	107.9	107.905	6	14	0.36
2	-	106.1	106.149	6	12	0.33
3	24-70	106.0	106.012	7	12	0.31
4	19-34	105.8	105.913	7	13	0.33
5	47-69	102.3	102.322	7	12	0.31
6	24-70 19-34	105.6	105.738	8	13	0.34
7	24-70 47-69	102.1	102.115	7	13	0.36
8	24-70 19-34 47-69	101.9	101.764	7	13	0.36

TABLE VII
COMPARISON WITH SOLVERS IN MATPOWER

N	ECQ		PDIPM		MINOS
	iterations	time (s)	iterations	time (s)	time (s)
9	9	0.11	10	0.34	0.14
14	9	0.11	14	0.36	0.14
30	9	0.16	15	0.39	0.16
39	11	0.17	16	0.39	0.16
57	11	0.23	14	0.45	0.20
118	11	0.34	18	0.62	0.59
300	13	0.79	25	1.25	6.54
2383	21	11.95	32	10.27	-

eight cases were considered in [26]. The same cases were simulated using the ECQ-OPF technique. In case 1, the tap settings are set to their values in [40]. In case 2, the taps are allowed to vary by $\pm 10\%$ from the nominal value of 1 pu. Cases 3 through 8 include on top of the tap-changing transformers in case 2 UPFC devices located in the lines shown in column 2 of Table VI. In all cases, voltages are allowed to vary by $\pm 10\%$ and reactive power generation limits are set to the values in [40].

Table VI shows that 1) the ECQ-OPF results are in agreement with the SQP results in [26] and 2) the ECQ-OPF iterations remain relatively constant even with the different numbers and locations of UPFC devices. The SQP iterations in [26] also remain relatively unchanged with the different cases, however they do not account for the iterations of the QP solver.

The IEEE 118-bus test system was also tested with quadratic generation cost curves in the presence of three UPFC devices set to control bus voltage magnitudes and active and reactive power flows. The UPFC locations are given in [31]. The ECQ-OPF converged in 13 iterations and 0.34 s for the case without UPFC devices (case 1), and in 11 iterations and 0.31 s for the case with UPFC devices (case 2). Reference [31] required 13 interior-point iterations for case 2. The evolution of the duality gap for cases 1 and 2 is given in Fig. 8.

VI. COMPARISON WITH MATPOWER

A comparison was carried between the ECQ-OPF and two OPF solvers available under MATPOWER [33]. MATPOWER allows the use of several types of optimizers, which include MINOS [32] and PDIPM [17]. MINOS uses a projected augmented Lagrangian algorithm, whereas PDIPM is an implementation of a primal-dual interior-point method. Both algorithms are applied to the OPF problem formulated in polar coordinates. The performance of the MINOS-OPF and PDIPM-OPF (with default settings) was compared with that of the ECQ-OPF on several test systems with quadratic cost functions and transformer taps fixed at pre-specified values. The complete data sets for these systems are provided with the MATPOWER distribution files [33]. Table VII includes the computational requirements of each of the methods. A comparison of the values in Table VII shows that 1) the MINOS-OPF is suitable for smaller networks, 2) the ECQ-OPF requires less iterations as compared to the PDIPM-OPF, and 3) the ECQ-OPF requires less computational time than the PDIPM-OPF for all test systems except the 2383-bus network. However, this comparison has to take into account that the ECQ-OPF optimizer is programmed as an m-file whereas the MATPOWER solvers are coded as MEX (MATLAB Executable) files. MATLAB runs its m-files in an interpretive mode, i.e., it compiles and executes each command, once at a time. Significant time savings will be produced by a MEX file implementation of the ECQ-OPF solver.

Table VIII shows the performance of the ECQ-OPF when started from two different points: flat start and power flow solution. The results show that the number of iterations is similar and that the solutions are virtually identical. Table VIII also includes the maximum real and reactive power mismatches for each of the test systems. The mismatches were obtained first by deriving the voltage polar coordinates solution from the ECQ solution and second by evaluating the nonlinear real/reactive power injection equations. The results confirm that the ECQ-OPF produces solutions that conform to the classical OPF formulation. Even the largest mismatch values are within MATPOWER's default maximum constraint violation tolerance of 5×10^{-6}.

TABLE VIII
ECQ-OPF PERFORMANCE WITH DIFFERENT STARTING POINTS

N	Starting Point: Flat			Starting Point: PF solution		
	iter.	ΔP_∞ (pu)	ΔQ_∞ (pu)	iter.	ΔP_∞ (pu)	ΔQ_∞ (pu)
9	9	3.1e-14	1.5e-14	8	1.2e-11	7.8e-12
14	9	4.4e-14	6.6e-14	9	4.4e-14	1.2e-13
30	9	1.7e-13	4.1e-13	8	2.5e-11	6.3e-11
39	11	2.0e-13	3.8e-13	10	1.1e-13	3.7e-13
57	11	8.6e-14	2.1e-14	11	1.2e-12	4.6e-13
118	11	1.3e-13	2.5e-13	11	8.6e-14	1.9e-13
300	13	2.6e-12	3.2e-12	12	4.0e-12	5.0e-12
2383	21	2.3e-07	1.7e-06	24	4.8e-06	1.6e-06

VII. CONCLUSION

This paper presented an OPF implementation which employs an extended conic quadratic load flow equations format as opposed to other classical formats which are based on the voltage polar coordinates model and the voltage rectangular model. The proposed format accounts for load flow controllers (tap-changing transformers, phase-shifting transformers, and UPFC devices) through their power injection models. The nonlinear constraints in the ECQ-OPF are limited to rotated conic quadratic and arctangent equalities. All other constraints are linear. This results in an OPF model that can be easily integrated in optimization functions that require the evaluation of second-order derivatives. A primal-dual interior-point method was chosen as the OPF solver because of its known robustness and efficiency in solving conic quadratic optimization problems. Numerical results and comparisons with previous research show that the proposed approach is promising.

APPENDIX A

To compute the Jacobian and Lagrangian Hessian matrices corresponding to (8), it is first rewritten as

$$f = R_{in}^2 + T_{in}^2 - 2u_i u_n.$$

The Jacobian and Hessian elements are

$$\frac{\partial f}{\partial R_{in}} = 2R_{in}, \frac{\partial f}{\partial T_{in}} = 2T_{in}, \frac{\partial f}{\partial u_i} = -2u_n, \frac{\partial f}{\partial u_n} = -2u_i$$
$$\frac{\partial^2 f}{\partial R_{in}^2} = \frac{\partial^2 f}{\partial T_{in}^2} = 2, \frac{\partial^2 f}{\partial u_n \partial u_i} = \frac{\partial^2 f}{\partial u_i \partial u_n} = -2.$$

Similarly, (9) is rewritten as

$$g = \theta_i - \theta_n - \tan^{-1}\frac{T_{in}}{R_{in}}.$$

The corresponding Jacobian and Hessian elements are

$$\frac{\partial g}{\partial \theta_i} = 1, \frac{\partial g}{\partial \theta_n} = -1, \frac{\partial g}{\partial R_{in}} = \frac{T_{in}}{R_{in}^2 + T_{in}^2}$$
$$\frac{\partial g}{\partial T_{in}} = \frac{-R_{in}}{R_{in}^2 + T_{in}^2}, \quad \frac{\partial^2 g}{\partial R_{in}^2} = \frac{-2R_{in}T_{in}}{(R_{in}^2 + T_{in}^2)^2}$$
$$\frac{\partial^2 g}{\partial T_{in}^2} = \frac{2R_{in}T_{in}}{(R_{in}^2 + T_{in}^2)^2}$$
$$\frac{\partial^2 g}{\partial R_{in}\partial T_{in}} = \frac{\partial^2 g}{\partial T_{in}\partial R_{in}} = \frac{R_{in}^2 - T_{in}^2}{(R_{in}^2 + T_{in}^2)^2}.$$

TABLE IX
GENERATOR DATA OF THE FIVE-BUS BENCHMARK EXAMPLE

Bus-i	$P_{gi}^{\min}$ [MW]	$P_{gi}^{\max}$ [MW]	$Q_{gi}^{\min}$ [MVAR]	$Q_{gi}^{\max}$ [MVAR]	c_{0i} [$/h]	c_{1i} [$/MWh]	c_{2i} [$/MW²h]
1	10	200	-300	300	60	3.4	0.004
2	10	200	-300	300	60	3.4	0.004

*100 MVA base

TABLE X
LINE DATA OF THE FIVE-BUS BENCHMARK EXAMPLE

Bus-i	Bus-j	r [pu]	x [pu]	$b_{sh}/2$ [pu]
1	2	0.02	0.06	0.03
1	3	0.08	0.24	0.025
2	3	0.06	0.18	0.02
2	4	0.06	0.18	0.02
2	5	0.04	0.12	0.015
3	4	0.01	0.03	0.01
4	5	0.08	0.24	0.025

TABLE XI
BUS DATA OF THE FIVE-BUS BENCHMARK EXAMPLE

Bus-i	Type	P_{di} [MW]	Q_{di} [MVAR]	$V_i^{\min}$ [pu]	$V_i^{\max}$ [pu]
1	Slack	0	0	0.9	1.5
2	PV	20	10	0.9	1.1
3	PQ	45	15	0.9	1.1
4	PQ	40	5	0.9	1.1
5	PQ	60	10	0.9	1.1

Because R_{in} is constrained to be nonnegative, the interior-point solver insures that R_{in} does not hit the exact boundary of zero at any iteration. Consequently, $R_{in}^2 + T_{in}^2 > 0$ and the Jacobian and Hessian elements are well defined. In practice, the primal and dual feasibility constraints are gradually satisfied as the solution point is approached, and in view of (8), $R_{in}^2 + T_{in}^2$ will always be well above zero.

APPENDIX B

Tables IX–XI show the generator data, line data, and bus data, respectively.

REFERENCES

[1] J. Carpentier, "Contribution a L'étude Du Dispatching Économique," in *Bulletin de la Société Française des Electriciens*, Aug. 1962, vol. III, pp. 431–447, ser. 8.

[2] D. I. Sun, B. Ashley, B. Brewer, A. Hughes, and W. F. Tinney, "Optimal power flow by Newton approach," *IEEE Trans. Power App. Syst.*, vol. PAS-103, pp. 2864–2880, Oct. 1984.

[3] R. C. Burchett, H. H. Happ, and D. R. Vierath, "Quadratically convergent optimal power flow," *IEEE Trans. Power App. Syst.*, vol. PAS-103, pp. 3267–3275, Nov. 1984.

[4] O. Alsac, J. Bright, M. Prais, and B. Stott, "Further developments in LP-based optimal power flow," *IEEE Trans. Power Syst.*, vol. 5, no. 3, pp. 697–711, Aug. 1990.

[5] A. M. Chebbo and M. R. Irving, "Combined active and reactive dispatch—Part 1: Problem formulation and solution algorithms," *Proc. Inst. Elect. Eng., Gen., Transm., Distrib.*, vol. 142, no. 4, pp. 393–400, Jul. 1995.

[6] R. Salgado, A. Brameller, and P. Aitchison, "Optimal power flow solutions using the projection method—Part 1: Theoretical basis," *Proc. Inst. Elect. Eng., Gen., Transm., Distrib.*, vol. 137, no. 6, pp. 424–428, Nov. 1990.

[7] S. J. Wright, *Primal Dual Interior Point Methods*. Philadelphia, PA: SIAM, 1997.

[8] S. Granville, "Optimal reactive dispatch through interior-point methods," *IEEE Trans. Power Syst.*, vol. 9, no. 1, pp. 136–146, Feb. 1994.
[9] Y. C. Wu, A. S. Debs, and R. E. Marsten, "A direct nonlinear predictor-corrector primal-dual interior-point algorithm for optimal power flows," *IEEE Trans. Power Syst.*, vol. 9, no. 2, pp. 876–883, May 1994.
[10] H. Wei, H. Sasaki, J. Kubokawa, and R. Yokoyama, "An interior point nonlinear programming for optimal power flow problems with a novel data structure," *IEEE Trans. Power Syst.*, vol. 13, no. 3, pp. 870–877, Aug. 1998.
[11] G. L. Torres and V. H. Quintana, "An interior-point method for nonlinear optimal power flow using voltage rectangular coordinates," *IEEE Trans. Power Syst.*, vol. 13, no. 4, pp. 1211–1218, Nov. 1998.
[12] R. A. Jabr, "A primal-dual interior-point method to solve the optimal power flow dispatching problem," *Optim. Eng.*, vol. 4, pp. 309–336, 2003.
[13] F. Capitanescu, M. Glavic, D. Ernst, and L. Wehenkel, "Interior-point based algorithms for the solution of optimal power flow problems," *Elect. Power Syst. Res.*, vol. 77, no. 5–6, pp. 508–517, Apr. 2007.
[14] G. L. Torres and V. H. Quintana, "On a nonlinear multiple-centrality-corrections interior-point method for optimal power flow," *IEEE Trans. Power Syst.*, vol. 16, no. 2, pp. 222–228, May 2001.
[15] W. Min and L. Shengsong, "A trust region interior point algorithm for optimal power flow problems," *Elect. Power Energy Syst.*, vol. 27, no. 4, pp. 293–300, May 2005.
[16] M. J. Rider, V. L. Paucar, and A. V. Garcia, "Enhanced higher-order interior-point method to minimise active power losses in electric energy systems," *Proc. Inst. Elect. Eng., Gen., Transm., Distrib.*, vol. 151, no. 4, pp. 517–525, Jul. 2004.
[17] H. Wang, C. E. Murillo-Sánchez, R. D. Zimmerman, and R. J. Thomas, "On computational issues of market-based optimal power flow," *IEEE Trans. Power Syst.*, vol. 22, no. 3, pp. 1185–1193, Aug. 2007.
[18] J. A. Momoh, M. E. El-Hawary, and R. Adapa, "A review of selected optimal power flow literature to 1993—Part I: Non-linear and quadratic programming approaches," *IEEE Trans. Power Syst.*, vol. 14, no. 1, pp. 96–104, Feb. 1999.
[19] J. A. Momoh, M. E. El-Hawary, and R. Adapa, "A review of selected optimal power flow literature to 1993—Part II: Newton, linear programming and interior-point methods," *IEEE Trans. Power Syst.*, vol. 14, no. 1, pp. 105–111, Feb. 1999.
[20] X.-P. Zhang, C. Rehtanz, and B. Pal, *Flexible AC Transmission Systems—Modelling and Control*. Berlin, Germany: Springer, 2006.
[21] N. S. Rau, "Issues in the path toward an RTO and standard markets," *IEEE Trans. Power Syst.*, vol. 18, no. 1, pp. 435–443, May 2003.
[22] X.-P. Zhang, S. G. Petoussis, and K. R. Godfrey, "Nonlinear interior-point optimal power flow method based on a current mismatch formulation," *Proc. Inst. Elect. Eng., Gen., Transm., Distrib.*, vol. 152, no. 6, pp. 795–805, Nov. 2005.
[23] R. A. Jabr, "A conic quadratic format for the load flow equations of meshed networks," *IEEE Trans. Power Syst.*, vol. 22, no. 4, pp. 2285–2286, Nov. 2007.
[24] A. G. Expósito and E. R. Ramos, "Reliable load flow technique for radial distribution networks," *IEEE Trans. Power Syst.*, vol. 14, no. 3, pp. 1063–1069, Aug. 1999.
[25] R. A. Jabr, "Radial distribution load flow using conic programming," *IEEE Trans. Power Syst.*, vol. 21, no. 3, pp. 1458–1459, Aug. 2006.
[26] E. Handschin and C. Lehmköster, "Optimal power flow for deregulated systems with FACTS devices," in *Proc. 13th Power Systems Computation Conf.*, Trondheim, Norway, Jun.-Jul. 1999, pp. 1270–1276.
[27] C. Lehmköster, "Security constrained optimal power flow for an economical operation of FACTS-devices in liberalized energy markets," *IEEE Trans. Power Del.*, vol. 17, no. 2, pp. 603–608, Apr. 2002.
[28] L. B. Tosovic, "Some experiments on sparse sets of linear equations," *SIAM J. App. Math.*, vol. 25, no. 2, pp. 142–148, Sep. 1973.
[29] E. Acha, C. R. Fuerte-Esquivel, H. Ambriz-Pérez, and C. Angeles-Camacho, *FACTS: Modeling and Simulation in Power Networks*. Chichester, U.K.: Wiley, 2004.
[30] O. Alsac and B. Stott, "Optimal load flow with steady-state security," *IEEE Trans. Power App. Syst.*, vol. PAS-93, pp. 745–751, May/Jun. 1974.
[31] X.-P. Zhang and E. J. Handschin, "Advanced implementation of UPFC in a nonlinear interior-point OPF," *Proc. Inst. Elect. Eng., Gen., Transm., Distrib.*, vol. 148, no. 5, pp. 489–496, Sep. 2001.
[32] B. A. Murtagh and M. A. Saunders, MINOS 5.5 User's Guide, Stanford Univ. Systems, Optimization Laboratory Tech. Rep. SOL 83-20R.
[33] R. D. Zimmerman and C. E. Murillo-Sánchez, MATPOWER 3.2 User's Manual, 2007. [Online]. Available: http://www.pserc.cornell.edu/matpower/.
[34] H. Saadat, *Power System Analysis*. Singapore: McGraw-Hill, 1999.
[35] E. D. Andersen, C. Roos, and T. Terlaky, On Implementing a Primal-Dual Interior-Point Method for Conic Quadratic Optimization, Optimization Online, 2000. [Online]. Available: http://www.optimization-online.org/DB_HTML/2000/12/245.html.
[36] H. Ambriz-Pérez, E. Acha, C. R. Fuerte-Esquivel, and A. De la Torre, "Incorporation of a UPFC model in an optimal power flow using Newton's method," *Proc. Inst. Elect. Eng., Gen., Transm., Distrib.*, vol. 145, no. 3, pp. 336–344, May 1998.
[37] J. M. R. Muñoz and A. G. Expósito, "A line-current measurement based state estimator," *IEEE Trans. Power Syst.*, vol. 7, no. 2, pp. 513–519, May 1992.
[38] R. A. Jabr, "Primal-dual interior-point approach to compute the L_1 solution of the state estimation problem," *Proc. Inst. Elect. Eng., Gen., Transm., Distrib.*, vol. 152, no. 3, pp. 313–320, May 2005.
[39] A. D. Belegundu and T. R. Chandrupatla, *Optimization Concepts and Applications in Engineering*. Englewood Cliffs, NJ: Prentice-Hall, 1999, p. 186.
[40] Power Systems Test Case Archive, Univ. Washington. [Online]. Available: http://www.ee.washington.edu/research/pstca/.

Rabih A. Jabr (M'02) was born in Lebanon. He received the B.E. degree in electrical engineering (with high distinction) from the American University of Beirut, Beirut, Lebanon, in 1997 and the Ph.D. degree in electrical engineering from the Imperial College (University of London), London, U.K., in 2000.

Currently, he serves as the Chairperson of the Electrical, Computer, and Communication Engineering Department at Notre Dame University, Zouk Mosbeh, Lebanon. His research interests are in mathematical optimization techniques, design optimization, optimal power flow, and state estimation.

Dr. Jabr received the Eryl Cadwaladar Davies Prize (2000) from the Imperial College and the Sebastien De Ferranti Premium Award (2003) from the Institution of Electrical Engineers (U.K.) for his work on optimal security dispatch.